

# All-Soft and Stretchable Thermogalvanic Gel Fabric for Antideformity Body Heat Harvesting Wearable

Tianpeng Ding, Yi Zhou, Xiao-Qiao Wang, Chen Zhang, Tongtao Li, Yin Cheng, Wanheng Lu, Jiaqing He, and Ghim Wei Ho\*

Currently, “wearable thermal-electric harvester” is a loose term for technology that embraces rigid thermoelectric leg incorporated flexible substrates. In reality, they are not exclusively flexible, much less totally soft and stretchable. Likewise, conventional substrate-dependent thermogalvanic cells lack the highly sought after mechanical adaptability, and hinder the full exploitation of the inherent merit of their fluidic matrices. The existence of the substrate causes poor air permeability and worse still, leads to low heat transfer efficiency. Here, a soft and stretchable thermogalvanic fabric directly woven out of p/n alternating hydrogel-based fibers is proposed. In addition to improved wearing comfort, the compliant mechanical properties of the thermogalvanic fabric possess desired adaptability to irregular and continuously deformed skin, so as to realize conformal and efficient body heat harvesting. The scalable and modular, processable soft gel serves as the groundwork to the realization of prototypical arbitrary fabric design and potentially a new battery-free bodily heat harvesting wearable.

battery-based energy supply systems, which require regular charging and raise concerns on waste disposal.<sup>[1–4]</sup> In this context, extensive efforts have been devoted to new energy harvesting strategies from ubiquitous yet overlooked environmental energy sources, such as piezoelectric generator,<sup>[5,6]</sup> triboelectric generator,<sup>[7,8]</sup> solar cell,<sup>[9,10]</sup> evaporation-driven generator,<sup>[11–13]</sup> moisture-driven generator,<sup>[14–16]</sup> etc. These energy supply methods have benefits of maintenance-free and eco-friendliness, especially suitable for decentralized energy demands in IoT. Among them, generators that directly convert thermal energy into electricity have the advantages of independence from the discontinuous mechanical movement or day-night alternation.<sup>[17,18]</sup> This lends to superiority for wearable electronics applications given

the ever present temperature difference between body and the environment.<sup>[19,20]</sup> Moreover in scenarios when there are occurrences of air convection, lower surrounding temperature, or increased activity of the users, one can anticipate considerably improved energy harvesting.

As one of the state-of-art thermal energy converting method, thermoelectric (TE) materials enable direct conversion of heat to electricity based on Seebeck effect. This effect originates from the temperature gradient driven diffusion of charge carriers.<sup>[21–23]</sup> However, traditional bulky and rigid TE materials are less suited for wearable systems. On the contrary, thermogalvanic cell (thermocell), which utilizes the temperature-dependent entropy changes during electron transfer between redox couples and electrodes, is intrinsically fluid and soft.<sup>[21]</sup> Moreover, the optimal operation temperature for common thermocell is less than 100 °C, unlike the much higher temperature for the TE counterparts, making it particularly relevant for daily scenarios.<sup>[24,25]</sup> Recently, significant advances and new insights have been made in the thermogalvanic heat conversion, leading a new upsurge of research in this area.<sup>[26–30]</sup> Nevertheless, most thermocells, if not all, have adopted hard and inelastic substrates to support the liquid working medium. As a consequence, their merits of softness and stretchability are overshadowed. Moreover, poor permeability of the devices with substrates affects the wearing comfortableness and causes health concerns in long-term wearing.

Hydrogel, a network of crosslinked hydrophilic polymer chains dominated by water constituent, is a promising

## 1. Introduction

The constantly escalating energy crisis and environmental pollution have necessitated ever-improving energy conversion technologies. Meanwhile, the huge and growing numbers of discrete electronics in the booming Internet of Things (IoT) are imperative to rid the dependence on the traditional

T. Ding, Y. Zhou, X.-Q. Wang, C. Zhang, T. Li, Y. Cheng, W. Lu, G. W. Ho  
Department of Electrical and Computer Engineering  
National University of Singapore  
Singapore 117583, Singapore  
E-mail: elehgw@nus.edu.sg

Y. Zhou, J. He  
Department of Physics  
Southern University of Science and Technology  
Shenzhen 518055, China

G. W. Ho  
Department of Materials Science and Engineering  
National University of Singapore  
Singapore 117575, Singapore

G. W. Ho  
Institute of Materials Research and Engineering  
A\*STAR (Agency for Science, Technology and Research)  
Singapore 117602, Singapore

 The ORCID identification number(s) for the author(s) of this article can be found under <https://doi.org/10.1002/aenm.202102219>.

DOI: 10.1002/aenm.202102219

candidate for wearable electronics for its tissue-like properties.<sup>[31–34]</sup> Herein, we propose a hydrogel-based heat harvesting fabric directly woven out of monolithic p/n alternating thermogalvanic fibers, so as to fully exploit the advantages of liquid thermocell whilst avoiding the air permeability flaw. To construct such thermogalvanic fibers, p-type and n-type hydrogel segments are sequentially bonded by inert composite electrodes via a modular assembly approach, while a thin soft coating serves as a protective layer, forming an all-soft material system. Beyond that, the thermogalvanic fiber inherits superior stretchability and elasticity of its components, imparting the much desired close materials interfacing between device and body with high mechanical performance. Notably, in addition to wearing comfort, this first proposed thermogalvanic fabric interlocked by such gel fibers possesses both stretchability and conformability. Distinguishing from the substrate-dependent counterparts, more importantly, it is endowed with capability to harvest body heat on irregular and repeatedly distorted skin surfaces, generating open-circuit voltages of around 0.7 V in cold ambient and up to 0.5 V on dynamic elbow. The scalability and

modularity of the fabricating strategy will provide a universal substrate-free approach to design stretchable and conformable thermogalvanic textile, promisingly open a new avenue for autonomous bodily heat harvesting wearables.

## 2. Results

The p/n alternating thermogalvanic fiber was fabricated through a modular processable approach, as illustrated in **Figure 1A**. To fabricate thermogalvanic hydrogel fibers, pure polyacrylamide (PAAm) hydrogel fibers were first freeze-dried and cut into aerogel segments with identical length. Then, the segmented aerogel modules were bonded with polydimethylsiloxane (PDMS)/carbon nanotube (CNT) composite in sequence (details are in the Experimental Section). The optical images of the assembled aerogel fibers are shown in the inset of **Figure 1A** and **Figure S1A** (Supporting Information), where white aerogel segments are uniformly connected to black PDMS/CNT electrodes. Subsequently, aqueous thermogalvanic electrolytes

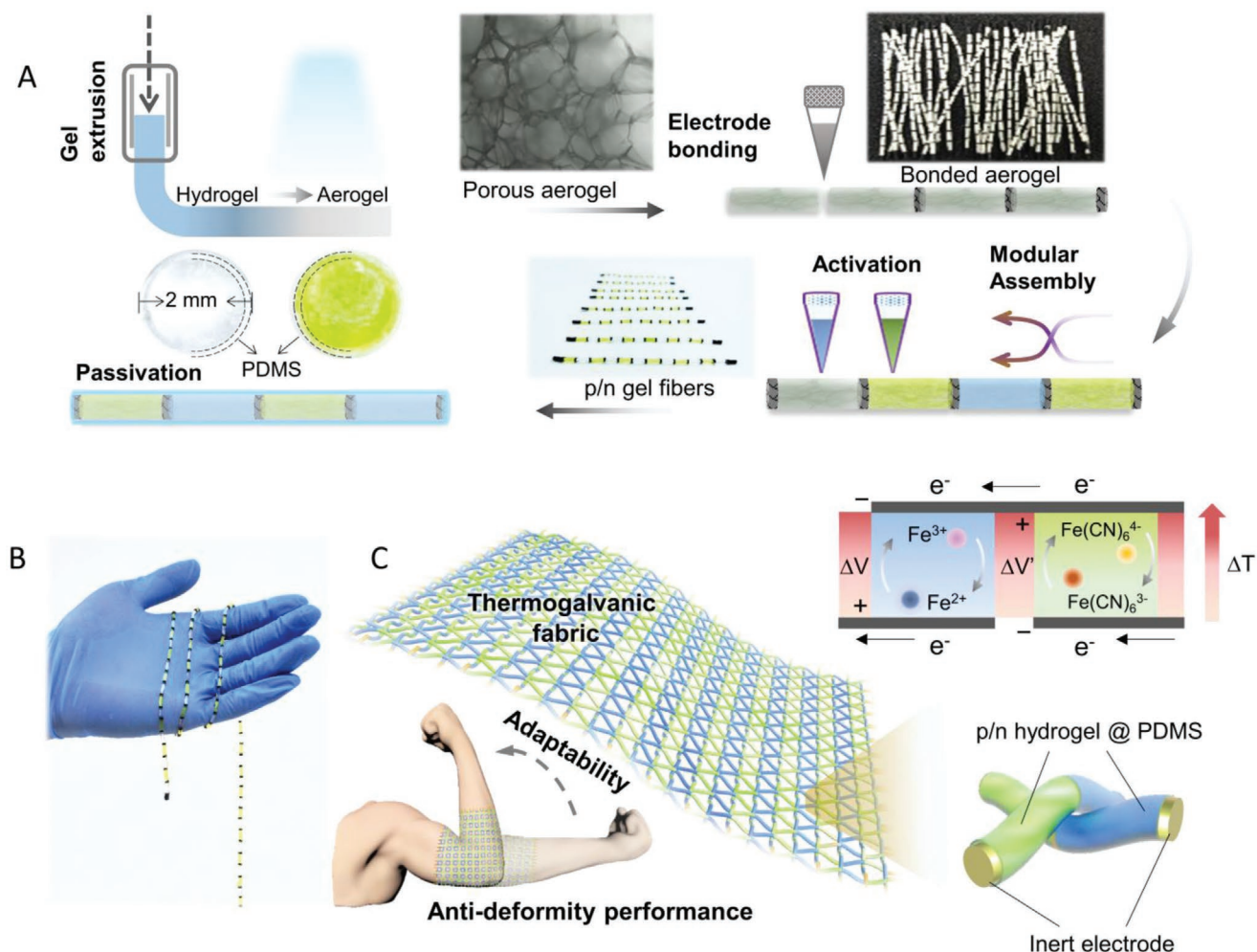


**Figure 1.** Wearable thermogalvanic body heat harvester. A) Schematic illustration of the modular fabrication process for p/n alternating thermogalvanic fibers. B) Optical image of a 1 m long hydrogel fiber. C) Soft and stretchable thermogalvanic fabric woven out of p/n alternating hydrogel-based fibers. PDMS/CNT composites are used as inert electrodes to bond the hydrogel segments and thin PDMS coating is coated on the fiber as passivation layer. Inset shows the schematic diagram of the body heat conversion for the weaving fiber containing p-type and n-type thermogalvanic redox couples.

containing p-type and n-type redox couples were alternatively added to the aerogel segments, endowing them with temperature relevant chemical reactivity. Here, the p-type and n-type thermogalvanic electrolytes are composed of aqueous solutions containing redox couples, namely  $\text{Fe}(\text{CN})_6^{3-}/\text{Fe}(\text{CN})_6^{4-}$  and  $\text{Fe}^{2+}/\text{Fe}^{3+}$ , respectively. Moreover, a thin layer of PDMS coating was used to encapsulate the hydrogel fiber to serve as protective barrier and provide a comfortable tactile sensation. The cross-sectional profiles of the n-type and p-type hydrogel segments are shown in the inset of Figure 1A. It can be seen that the cylindrical hydrogel cores are fully soaked and colored with electrolytes (the pale one is n-type and the yellow one is p-type), and the outside surfaces are uniformly coated with thin PDMS layers. The prepared monolithic p/n alternating thermogalvanic fiber is presented in Figure 1B, where p-type and n-type segments form a bamboo-like structure. The superior water-holding capacity of PAAm hydrogel is derived from its porous construct made up of polymer walls, as shown in Figure S1B (Supporting Information). Such porous open-cell structure provides the electrolyte with both the matrix to maintain the shape and the redox pathways for exchange reactions.

To construct the hydrogel-based thermogalvanic textile, p/n alternating thermogalvanic fibers are regularly interlaced, with joint electrodes periodically and alternatively situated at opposite sides of the fabric. Figure 1C schematically presents the illustration of the soft and stretchable textile, with antideformity

and highly adaptive conformable body heat harvesting. The inset of Figure 1C reveals the detail of the weaving structure. The PDMS/CNT composites that bond the gel segments also serve as nonreactive inert electrodes, so as to collect and transfer the electrons during redox reaction. When the fabric is placed on the skin, temperature gradient will be established along each thermogalvanic segment in the weaving fibers. With p/n type hydrogel segments sequentially alternating in each fiber, the temperature gradient induced electrons will flow in the same direction along the fiber. Thus, the thermogalvanic fabric is judiciously connected in parallel thermally and in series electrically, which has been demonstrated to be the optimal geometrical configuration.

To coat the PDMS passivation layer, a silane-assisted method reported previously was used to engender a firm bond to the gels.<sup>[35]</sup> Peeling test (inset in Figure 2A) presents a peel force of over  $100 \text{ N m}^{-1}$ , as shown in Figure 2A, indicating the well bonded interface. By virtue of their superior mechanical properties, both PDMS and PAAm hydrogel have been widely tested and implemented in wearable electronics. We performed tensile tests for p-type segment, n-type segment and p/n alternating fiber, with all the samples coated with PDMS. Figure 2B presents the tensile stress–strain curves, showcasing similar characteristics reaching ultimate strains of  $\approx 170\%$  with corresponding stress of  $\approx 50 \text{ kPa}$ . Compared with the stress–strain curves of the pure PAAm hydrogel (Figure S2A, Supporting

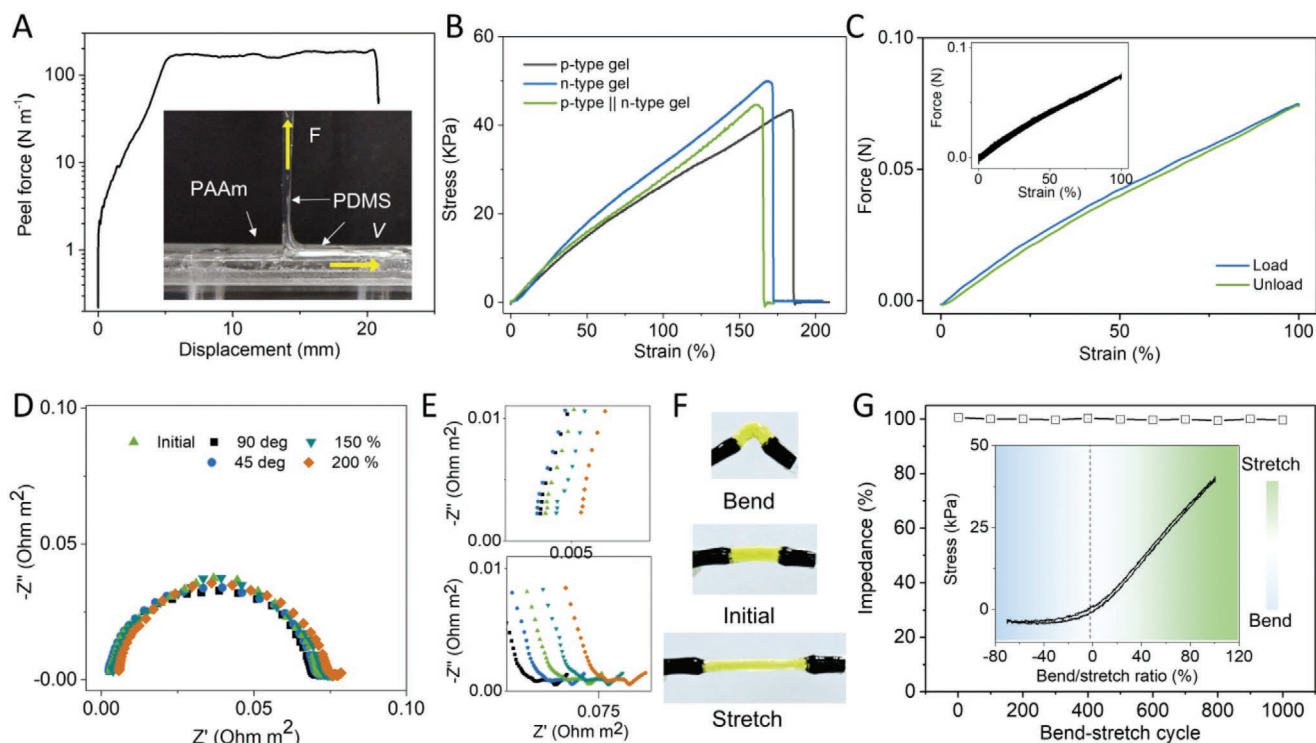


**Figure 2.** Mechanical properties of thermogalvanic fibers. A) Curve of the peel force verse displacement between the PDMS and hydrogel. Inset is the photo of the interface between the PDMS and PAAm hydrogel during peel force test. B) Stress–strain curves for the unitary n-type hydrogel fiber, unitary p-type hydrogel fiber and p/n alternating hydrogel fiber. C) Loading–unloading test of the p/n alternating fiber. Inset is the repeating test of 1000 cycles. D) Electrochemical impedance spectra of a 5 mm p-type segment with different deformation, including being compressive bended to 90° and 45°, initial state, stretched to be 150% and 200% of its initial length. E) Partially enlarged images of (D). F) Photos for p-type hydrogel segment at bend, initial and stretch states. G) Stability test of the impedance of the p-type hydrogel segment during 1000 bend–stretch cycles. Inset shows the stress–strain curve of the fiber during one bend–stretch period.

Information), the PDMS coated samples exhibit higher tensile strength benefitting from the much tougher PDMS layer (Figure S2B, Supporting Information). The consistency in the mechanical properties of the p/n alternating fiber to that of the solitary p-type or n-type fibers indicates sufficient interconnecting strength between the adjacent segments. Also, the composite electrodes are designed to possess good stretchability to ascertain the totality in mechanical compliance (Figure S2C, Supporting Information). Other conductive composites using conductive fillers and stretchable polymers are also suitable in this system.<sup>[36–38]</sup> It is noteworthy that the Young's moduli of the thermogalvanic gel fibers are comparable to the biological tissue (<100 kPa), thus they can offer the desirable fabric softness that is comfortable to wear next to the skin. Loading-unloading tests of 100% strain were conducted to test stretchability of the thermogalvanic fibers (Figure 2C, Figure S3, Supporting Information), which exhibit slight hysteresis, suggesting little energy dissipation occurs during the process. The overlapping stress-strain curves of the 1000 cycles of repetitive loading test further demonstrate their superior mechanical stretchability and elasticity, as shown in the Figure 2C inset.

For a typical thermocell, electricity generation performance is crucially affected by electrochemical factors, including interface kinetic, ion migration, electrode materials, and so on.<sup>[39]</sup> These factors in turn vary with device shape deformations, a scenario identified in wearable electronics application, which can give rise to variations in energy generation output. Hence, we performed electrochemical impedance spectroscopy (EIS) test to assess the influence of shape deformations between compressed bending and stretching, as shown in Figure 2D and Figure S4A (Supporting Information). The EIS presents inconsiderable difference when the bending angle and stretching ratio are at 90° and 100% respectively. Enlarged EIS spectra in Figure 2E reveal slightly increased impedances in low-frequency region as the gel is stretched, which is mainly attributed to the increase in PDMS/CNT composite electrode resistance when stretched (Figure S5, Supporting Information). Different from the stretching condition, compression induced bending reduces the impedances as the diffusion-limited mass transportation effect is reduced when ion exchanging path becomes shorter. Also, higher Young's modulus of the PDMS/CNT electrodes, which can ensure a constant electrochemical surface area during deformation, accounts for the nearly unchanged electrochemical conductivity. I-V curves of the samples at different bend/stretch states are in line with the trends of the EIS curves, as shown in Figures S4b,c and S6 (Supporting Information). Moreover, the relationship between conductivity and hydrogel segment length was also studied (Figure S7, Supporting Information), showing a much smaller change ratio for conductivity compared to the fiber length. Notably, this antideformation impedance change of the thermogalvanic fibers is favorable for stable energy generation performance in shape-changing conditions, which will discuss later. The photos for a p-type segment at different deformations status are shown in Figure 2F. Continuous and repeated bend-stretch tests are conducted on the hydrogel segments, as shown in Figure 2G and Figure S8 (Supporting Information), demonstrating robust and constant impedances. Inset in Figure 2G shows the stress evolution during a bend/stretch cycle. The superiority of both

mechanical and electrochemical properties of the thermogalvanic fibers lay the primary foundation for conformal heat harvesting.

The hydrogel containing redox couples exhibit p-type and n-type thermogalvanic Seebeck coefficients of 1.24 and  $-1.05 \text{ mV K}^{-1}$ , respectively, as shown in Figure 3A. The voltage performances are comparable with previously reported values.<sup>[26,40]</sup> It is reasonable that the current densities of the fibers are relatively smaller, since the ion diffusion in the confined hydrogel matrix is restrained and the resistance of the stretchable PDMS/CNT composite electrode is much larger compared to the rigid metal or graphite electrode (Figure S9, Supporting Information). Figure 3B and 3C exhibit the output voltage of the p-type and n-type segments with 5 mm length under different temperature differences, respectively. It can be seen that the open-circuit voltage of the load increase linearly with the temperature differences across the thermogalvanic segment from 5 to 20 K. Like any other typical electrochemical reaction based device, the performance of the thermocell is positively related to the electrode areas, similar to supercapacitor and electro-catalysis.<sup>[41–43]</sup> In our device, the PDMS/CNT composite infiltrates and percolates into the porous PAAm aerogel, as shown in Figure 3D and Figure S10A (Supporting Information). The embossed electrodes possess a much rougher surface, and thus bestow a large surface area (Figure 3E). Compared to usual planar electrodes, these embossed ones enable much higher electrochemical conductivity (Figure 3F and Figure S10B–D, Supporting Information). The higher electrochemical conductivity implies better interfacial reaction kinetics, guaranteeing larger thermogalvanic currents than the flat devices.

When temperature gradient is established between two terminals of a hydrogel segment, the temperature profiles will vary according to the subjected deformation. Figure 3G presents the evolution of the temperature profile of a hydrogel segment under different deformations. Here, the temperatures of the heating/cooling terminals are fixed at the two ends of the segments during the physical deformation testing. Remarkably, despite significant deformation of the hydrogel segments, the output performances of the thermogalvanic gel remain nearly unchanged, as indicated in Figure 3H. This unskewed thermogalvanic performance is consistent with the properties of electrochemical conductivity for the hydrogels discussed previously. Furthermore, continuous open-circuit voltage and load voltage of the thermogalvanic segments with different deformed shapes are recorded in Figure 3I and Figure S11 (Supporting Information), showing no obvious decrease on either of the voltages, which verifies the antideformity generating performance.

To test the out-of-plane heat harvesting performance, a hydrogel fiber composed of six pairs of p/n thermogalvanic segments were constructed, as shown in Figure 4A. The fiber is placed on a substrate with sequentially raised or lowered parts held by holders, so as to make the p/n joints alternatively top and bottom sections exposed. Inset shows the enlarged photo of a p/n pair. When the temperature of substrate is different from the ambient, temperature gradient will occur in the out-of-plane direction. Figure 4B shows the infrared image when the substrate and ambient temperature are at 32 and 22 °C, respectively. The corresponding temperature of the p/n joints

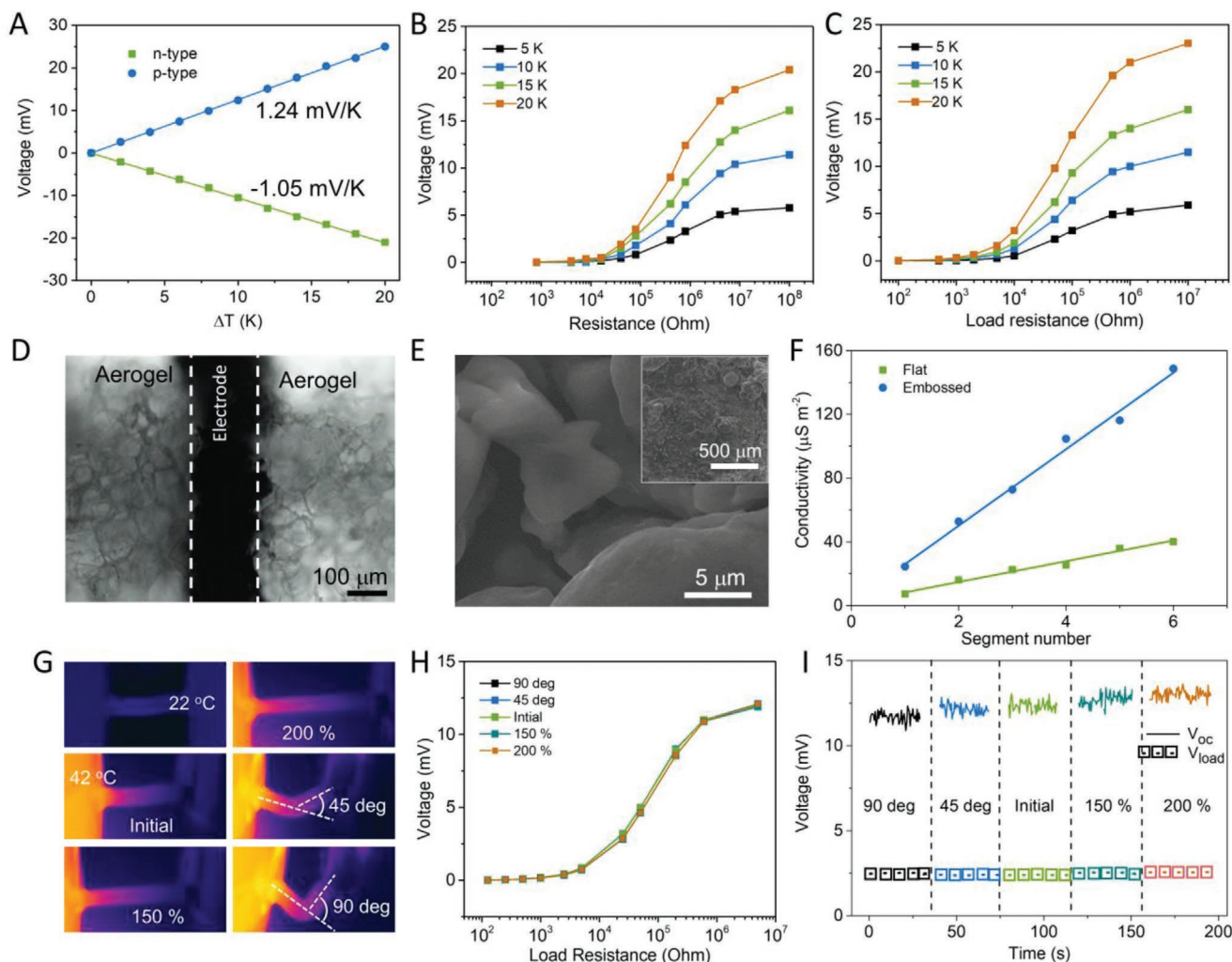


**Figure 3.** Electrical properties of the thermogalvanic fibers. A) Open-circuit voltage of the p-type and n-type segments at different temperature differences. Output voltage of the B) n-type and C) p-type hydrogel segments with different load resistances at different temperature differences. D) Optical microscope photo of the aerogel joint. Black PDMS/CNT composite is marked out by the brown dashed lines. E) SEM image of the embossed PDMS/CNT electrode. Inset is a wide view of a PDMS/CNT electrode. F) Conductivities of flat and embossed PDMS/CNT electrodes with different numbers of p-type hydrogel segments. G) Temperature profiles for hydrogel segments at no temperature difference, and temperature difference of 10 K with different deformations. H) Output voltages of a p-type hydrogel segment with different deformations at  $\Delta T = 10$  K. I) Continuous measurement of open-circuit voltage and load voltage ( $R = 20$  kohm) for a p-type hydrogel segment with different deformations. For all the measurement above, the length of the hydrogel segments is fixed at 5 mm.

are presented in Figure 4C, revealing a uniform and lower temperature distribution in the out-of-plane direction. Thus, a unidirectional electron flow is generated along the hydrogel fiber, in a mechanism described previously in Figure 1C. In order to test the performance of the individual p/n pair (denoted as 1–6) in a fiber, thin carbon wires were separately inserted in the PDMS/CNT electrodes. The  $I$ – $V$  curves of the segments without any temperature gradient are shown in Figure 4D and Figure S12 (Supporting Information), depicting a gradually increasing trend as the pair number increases. Inset of Figure 4D shows the approximate linear relation between the resistance and the pair number, of which the values are derived from Figure 4D. It can be seen that the cross points of the  $I$ – $V$  curves are at zero when there is no temperature difference between substrate and ambient. The different reaction areas of the embossed

PDMS/CNT electrodes primarily account for the discrepancy between the conductivities of the pairs. As temperature gradient is established, thermogalvanic open-circuit voltage and short-circuit current are generated, whose values can be derived from the intercepts of the  $I$ – $V$  curves on the horizontal and vertical coordinates, respectively. Figure S13 (Supporting Information) and Figure 4E show the  $I$ – $V$  curves and derived voltage/current values of every individual p/n pair when the temperature difference between substrate and ambient was 10 K. Each of the p/n pair generates thermogalvanic output of similar value. Since the p/n pairs are connected electrically in series along the fiber, the open-circuit voltage will multiply accordingly while the short circuit current remains almost unchanged, as shown in Figure 4F. Additionally, the performances of the fiber with different substrate temperatures were also tested as shown in

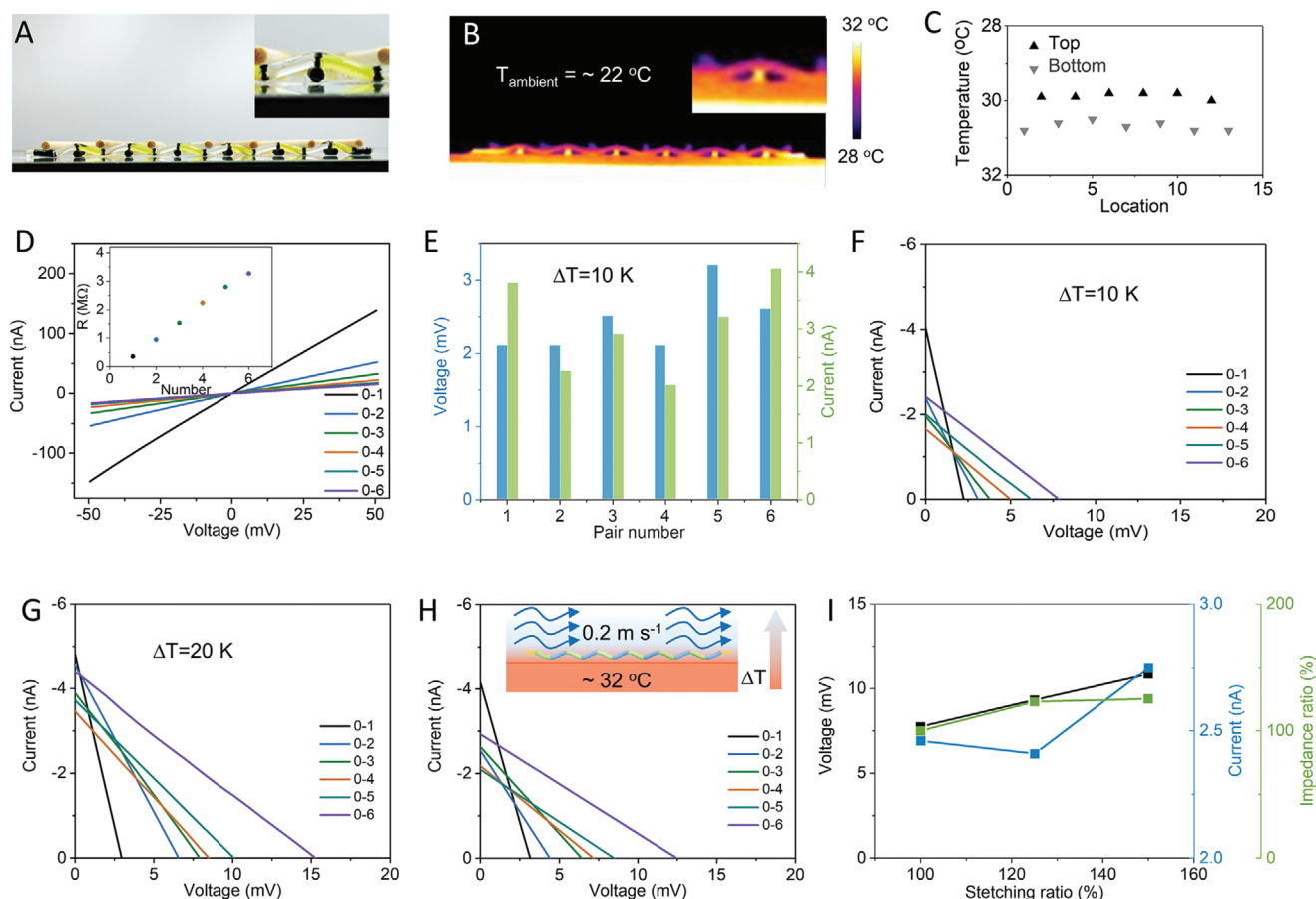


**Figure 4.** Heat harvesting for a p/n alternating thermogalvanic fiber in out-of-plane direction. A) Photo for the test set up of a hydrogel fiber with 6 p/n pairs, denoted as 1 to 6. The fiber is alternatively lifted or lowered in sequence at joint electrodes by holders. Inset is the enlarged photo showing the detail of a p/n pair. B) IR image of the fiber when the temperature of the substrate is 32 °C. Inset shows the enlarged IR image for a p/n pair. C) Temperature of the top (exposed to ambient) and bottom (close to substrate) joint electrodes. D) *I*–*V* curves of the numbered p/n segments. Inset is the relationship between the pair number and impedance derived from the slope of *I*–*V* curves. E) Open-circuit voltage and short-circuit current values of each p/n pair when substrate temperature is 32 °C. F–G) *I*–*V* curves of different numbers of p/n pairs when the substrate temperature is F) 32 °C and G) 42 °C. *I*–*V* curves of different numbers of segments when a gentle wind of 0.2 m s<sup>−1</sup> is applied with a substrate temperature of 32 °C. H) Performance of the hydrogel fibers as it is stretched to be 100%, 125%, and 150% of its initial length when the substrate is 32 °C. For all the tests above, the ambient is constant of around 22 °C.

Figure 4G and Figure S14 (Supporting Information). As the temperature difference increase from 5 to 20 K, the open-circuit voltage generated by the fiber also increases from ≈5 to ≈15 mV, accordingly. The temperature distribution is affected by various factors, for example, wind is one of the most common and obvious influence factors. A gentle breeze of around 0.2 m s<sup>−1</sup> was applied to the fiber to test the influence of wind on the thermogalvanic performance, as shown in Figure 4H. Both the voltage and current increase compared with the still air condition, signifying a potential and practical means of boosting heat harvesting, especially used in outdoor. Besides evaluating the energy harvesting performance in a relax state, the thermogalvanic fiber was also tested at different stretching ratio. As can be seen from Figure 4I and Figure S15 (Supporting Information), both of the open-circuit voltage and short-circuit current present slight increment when the fiber was stretched to 150%. It can be deduced from the observation that the taut fiber was moved farther apart by the holders and thus the air movement was enhanced which led to improved galvanic performance.

It is noteworthy that the impedance of the fiber only increases around 125%, a much smaller value compared to the common electronic conductor which will increase to 225%. It should be noted that, the PDMS layer with lower thermal conductivity will not only provide protection to the fiber, but is also favor of establishing higher temperature difference across the fiber.<sup>[44]</sup> Video in the Supporting Information shows the superior flexibility and stretchability of a thermogalvanic hydrogel fiber.

For wearable electronics, especially body heat harvesting, ergonomic compliance is a primary consideration toward good performance as well as human well-being. Benefitting from the superior flexibility of each individual fiber, the thermogalvanic fabric woven by the p/n alternating fibers are also flexible (detailed fabrication process is described in the Experimental Section). The flexibility of the fabric allows close contact to the skin on the curved surface which eliminates the heat shielding air gap, to fully harvest body heat, as schematically shown in Figure 5A. Moreover, gaps between the fibers in the fabric provide sufficient gas exchange path, endowing

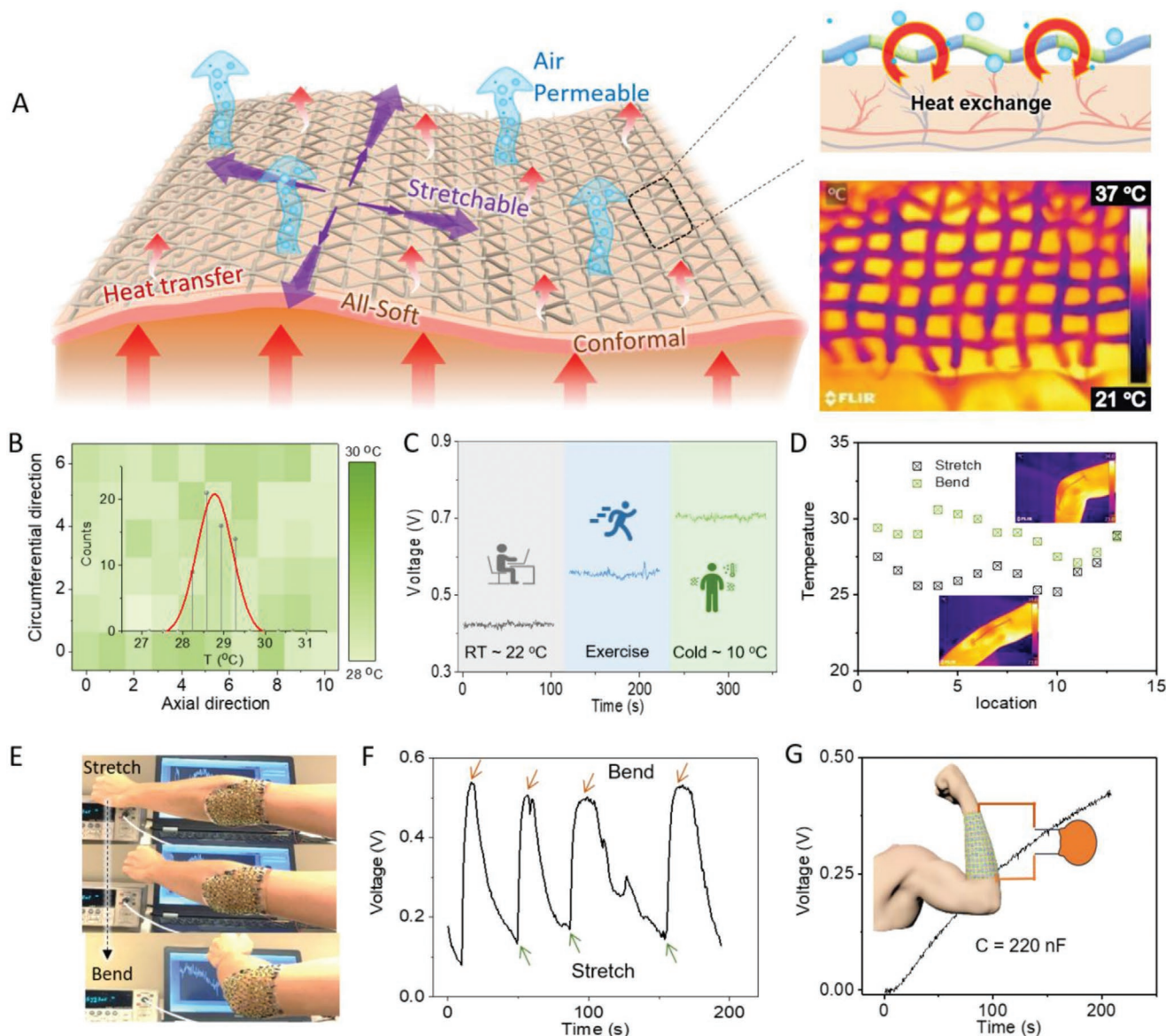


**Figure 5.** Conformal body heat harvesting of the thermogalvanic hydrogel fabric. A) Schematic illustration for wearable body heat harvesting. Insets are the diagram of bodily heat harvesting (top) and IR image of the thermogalvanic fabric worn on arm (bottom). B) Temperature distribution of the fabric joints derived from the IR images of (A). Inset is the statistical distribution of the temperature, showing a very narrow range between 28 and 30 °C. C) Open-circuit voltages of the thermogalvanic fabric worn on arm in different scenarios, including sitting still, after exercise and in cold ambient. D) Temperature evolution of a hydrogel fiber fixed on a moving elbow. The temperature data are acquired from the IR images at the joint electrodes location. E) Photos for the thermogalvanic fabric worn on arm at different bending movements. F) Open-circuit voltage of the device during continuous movement corresponding to (E). G)  $V$ - $T$  curves of a commercial ceramic capacitor of 220 nF charged by the thermogalvanic fabric worn on arm.

it with high permeability. The thermogalvanic fabric can be conformably wrapped on the arm (Figure S16A, Supporting Information) and the outer surface presents a lower yet uniform temperature profile, as indicated in the infrared image (inset of Figure 5A) and the corresponding temperature distribution profile (Figure 5B). The energy generation performances at different scenarios have also been studied, as shown in Figure 5C, indicating that higher skin temperature (after exercise) or cooler ambient temperature (in cold environment) is certainly beneficial for enhanced electricity generation, with an output voltage comparable to the reported highest wearable

body heat harvesters (Table S1, Supporting Information). Meantime, simulation results (Supporting Figure Simulation S1C, Supporting Information) also show that higher air heat exchange coefficient will benefit the device performance. In contrast to previously reported substrate-based thermogalvanic devices, the elastic fiber-woven fabric is able to accommodate stretching deformation of the skin. As indicated in Figure 5D, when attached at an elbow, not only has the temperature of the stretchable fiber not dropped, they have in fact increased to some extent. The temperature increase is associated to the closer contact to the stretched elbow skin when

the arm is bent, citing a potential for better performance. Figure 5E shows the photos of the thermogalvanic fabric worn at the elbow, showing a superior compliance when the arm is stretched or bent. The corresponding voltage signal during the movement is recorded in Figure 5F, which has clearly proven the superiority of the stretchability at body joint, relevant to wearable application. Furthermore, a commercial ceramic capacitor was charged up by an arm-wearing thermogalvanic fabric, as shown in Figure 5G, so as to demonstrate its practical application. We also perform the continuous test of the fabric wrapped around a beaker with gradually changed temperature (Figure S16B, Supporting Information), verifying its stable and consistent performance.

### 3. Conclusion

In conclusion, we propose a soft wearable thermogalvanic generator for body heat harvesting, having the advantages of exceptional stretchability and compliance. The generating modules are directly woven into fabric configuration by p/n alternating thermogalvanic fibers, completely ridding the dependence on air impermeable substrates, hence rendering it comfortable for long-term wearing. The adaptability of thermogalvanic fabric to irregular skin surface and continuous movements are also demonstrated, generating open-circuit voltages of around 0.7 V in cold ambient and up to 0.5 V on dynamic moving elbow. It is worth noting that the concepts presented in this work can also be scaled up and applied in other wearable thermogalvanic generators, and provide new inspiration for other fiber-based textile electronics.

### 4. Experimental Section

**Material Synthesis and Device Fabrication:** For PAAm aerogel fiber preparation: First, 10 g of acrylamide monomer (AM, >98%, TCI), 240 mg of *N,N'*-methylenebisacrylamide (MBA, 99%, Sigma-Aldrich), 100 mg of ammonium peroxydisulfate (APS, 98%, Sigma-Aldrich), and 100 mg of 3-(trimethoxysilyl)propyl methacrylate (TMSPMA, TCI, M0725) as silane coupling agent were mixed with 50 mL deionized (DI) water to prepare the precursor. Then the degassed precursor was polymerized in a PTFE tube with inner diameter of 1.6 mm at 80 °C for 15 min. After extruded from the tube, the PAAm hydrogel fibers were totally washed in DI water and subjected to freeze-drying process to form the PAAm aerogel fibers. For PDMS/CNT composite: 100 mg MWCNT (XFNANO, XFM03) and 1 g PDMS base (Dow Corning) were uniformly mixed in 100 mL Hexane anhydrous (95%, Sigma-Aldrich) with probe ultrasonication (150W, 20 KHz, SONICS) for 30 min. Then, 0.1 g curing agent (95%, Sigma-Aldrich) was added in the prepared mixture and ultrasonicated (150W, 20 KHz, SONICS) for another 30 min. Subsequently, the mixture was stirred and evaporated to form liquid PDMS/CNT composite. Part of the liquid PDMS/CNT composite was extruded from a syringe and cured in 80 °C oven to form solid PDMS/CNT rods. For p-type and n-type thermogalvanic electrolytes:  $K_3Fe(CN)_6$  (99%, Sigma-Aldrich) and  $K_3Fe(CN)_6 \cdot 3H_2O$  (98.5-102.0%, Sigma-Aldrich) were dissolved in DI water to form the p-type electrolyte of 0.1 M.  $FeCl_3$  (97%, Sigma-Aldrich) and  $FeCl_2$  (98%, Sigma-Aldrich) were dissolved in DI water to form the n-type electrolyte of 0.1 M.

To fabricate the p/n alternating thermogalvanic fibers, first, the PAAm aerogel fibers were cut into uniform segments with length of 5 mm. Then 12 aerogel segments were bonded one by one with the prepared liquid PDMS/CNT composite and the two terminals were bonded with solid PDMS/CNT rods. Afterward, the samples were cured in oven at

80 °C to be the aerogel fibers, as shown in the Figure S1A (Supporting Information). After that the aerogel fibers were immersed with DI water and restored to be hydrogel form. Then, 2  $\mu$ L of previously prepared p-type and n-type electrolyte were added on the segments alternatively, so as to chemically active p/n alternating thermogalvanic fibers. To coat PDMS layer on the hydrogel fibers, PDMS base and curing agent was mixed with triethoxyvinylsilane (TEOVS, TCI, V0044) (served as silane coupling agent with weight ratio of base: curing agent: silane = 10:1:0.1). Then the bare p/n alternating hydrogel fibers were dipped coating with the silane-contained PDMS precursor and cured in vacuum drying oven. Single p/n segment test were conducted by bonding the segments between two carbon paper strips with PDMS/CNT composite. The thermogalvanic fabric was woven by 24 p/n alternating fibers in uniform gaps to make the joints alternatively top and down, as shown in Figure 1C. To fix the fabric configuration, additional PDMS was used to bond the interlaced fibers at the cross nodes. The terminal electrodes of each fiber were connected with conductive wires to realize electrical connection in series. To mount the fabric on the body, transparent VHB double-sided tapes (3M) were first adhered on the external edge of the fabric. Then the fabric was adhered on the body in a spread out state. Then, another layer of Scotch tapes was covered on the external edge of the fabric to firmly fix it on the skin.

**Characterization and Tests:** The morphologies of the fibers were characterized by SEM (FESEM, JEOL FEG JSM 7001F) and microscope (Olympus, DP27). The tensile stress-strain test was implemented using force testing System (MultiTest-I, Mecmesin). During electrical performance test, two K-type thermocouples were used to record the temperature of the substrate and ambient. An Infrared camera (E50, FLIR Systems) was used to capture the infrared images. The open-circuit voltages were recorded by nanovoltmeter (Keithley 2182A). The IV curves and EIS of the samples were tested using an electrochemical workstation (CHI660E).

### Supporting Information

Supporting Information is available from the Wiley Online Library or from the author.

### Acknowledgements

This research was supported by the NUS Hybrid-Integrated Flexible (Stretchable) Electronic Systems Program grant number R-263-501-011-731. This work by the author(s) is partially/fully supported by the Advanced Research and Technology Innovation Centre (ARTIC). Informed consent was obtained from the participant prior to all relevant experiments.

### Conflict of Interest

The authors declare no conflict of interest.

### Data Availability Statement

The data that support the findings of this study are available from the corresponding author upon reasonable request.

### Keywords

body heat harvesting, hydrogels, thermogalvanics, wearable electronics

Received: July 21, 2021  
Revised: September 21, 2021  
Published online: October 13, 2021

- [1] Z. L. Wang, *Nano Today* **2010**, *5*, 512.
- [2] M. Haras, T. Skotnicki, *Nano Energy* **2018**, *54*, 461.
- [3] H. Ryu, H. J. Yoon, S. W. Kim, *Adv. Mater.* **2019**, *31*, 1802898.
- [4] M. Ye, Z. Zhang, Y. Zhao, L. Qu, *Joule* **2018**, *2*, 245.
- [5] Z. L. Wang, J. Song, *Science* **2006**, *312*, 242.
- [6] Y. Qin, X. Wang, Z. L. Wang, *Nature* **2008**, *451*, 809.
- [7] F. R. Fan, Z. Q. Tian, Z. L. Wang, *Nano Energy* **2012**, *1*, 328.
- [8] R. Hinchet, H. J. Yoon, H. Ryu, M. K. Kim, E. K. Choi, D. S. Kim, S. W. Kim, *Science* **2019**, *365*, 491.
- [9] G. Yu, J. Gao, J. C. Hummelen, F. Wudl, A. J. Heeger, *Science* **1995**, *270*, 1789.
- [10] Y. Liu, S. Akin, L. Pan, R. Uchida, N. Arora, J. V. Milić, A. Hinderhofer, F. Schreiber, A. R. Uhl, S. M. Zakeeruddin, A. Hagfeldt, M. I. Dar, M. Grätzel, *Sci. Adv.* **2019**, *5*, eaaw2543.
- [11] G. Xue, Y. Xu, T. Ding, J. Li, J. Yin, W. Fei, Y. Cao, J. Yu, L. Yuan, L. Gong, J. Chen, S. Deng, J. Zhou, W. Guo, *Nat. Nanotechnol.* **2017**, *12*, 317.
- [12] T. Ding, K. Liu, J. Li, G. Xue, Q. Chen, L. Huang, B. Hu, J. Zhou, *Adv. Funct. Mater.* **2017**, *27*, 1700551.
- [13] Z. Zhang, X. Li, J. Yin, Y. Xu, W. Fei, M. Xue, Q. Wang, J. Zhou, W. Guo, *Nat. Nanotechnol.* **2018**, *13*, 1109.
- [14] F. Zhao, H. Cheng, Z. Zhang, L. Jiang, L. Qu, *Adv. Mater.* **2015**, *27*, 4351.
- [15] H. Wang, Y. Sun, T. He, Y. Huang, H. Cheng, C. Li, D. Xie, P. Yang, Y. Zhang, L. Qu, *Nat. Nanotechnol.* **2021**, *16*, 811.
- [16] Y. Huang, H. Cheng, C. Yang, H. Yao, C. Li, L. Qu, *Energy Environ. Sci.* **2019**, *12*, 1848.
- [17] C. R. Bowen, J. Taylor, E. LeBoulbar, D. Zabek, A. Chauhan, R. Vaish, *Energy Environ. Sci.* **2014**, *7*, 3836.
- [18] X. L. Shi, J. Zou, Z. G. Chen, *Chem. Rev.* **2020**, *120*, 7399.
- [19] R. Tian, Y. Liu, K. Koumoto, J. Chen, *Joule* **2019**, *3*, 1399.
- [20] G. Chen, Y. Li, M. Bick, J. Chen, *Chem. Rev.* **2020**, *120*, 3668.
- [21] X. Shi, J. He, *Science* **2021**, *371*, 343.
- [22] B. Jiang, Y. Yu, J. Cui, X. Liu, L. Xie, J. Liao, Q. Zhang, Y. Huang, S. Ning, B. Jia, B. Zhu, S. Bai, L. Chen, S. J. Pennycook, J. He, *Science* **2021**, *371*, 830.
- [23] F. Kim, B. Kwon, Y. Eom, J. E. Lee, S. Park, S. Jo, S. H. Park, B.-S. Kim, H. J. Im, M. H. Lee, T. S. Min, K. T. Kim, H. G. Chae, W. P. King, J. S. Son, *Nat. Energy* **2018**, *3*, 301.
- [24] J. Duan, B. Yu, L. Huang, B. Hu, M. Xu, G. Feng, J. Zhou, *Joule* **2021**, *5*, 768.
- [25] K. Liu, Y. Zhou, F. Yuan, X. Mo, P. Yang, Q. Chen, J. Li, T. Ding, J. Zhou, *Angew. Chem., Int. Ed. Engl.* **2016**, *55*, 15864.
- [26] P. Yang, K. Liu, Q. Chen, X. Mo, Y. Zhou, S. Li, G. Feng, J. Zhou, *Angew. Chem., Int. Ed. Engl.* **2016**, *55*, 12050.
- [27] B. Yu, J. Duan, H. Cong, W. Xie, R. Liu, X. Zhuang, H. Wang, B. Qi, M. Xu, Z. L. Wang, J. Zhou, *Science* **2020**, *370*, 342.
- [28] C. G. Han, X. Qian, Q. Li, B. Deng, Y. Zhu, Z. Han, W. Zhang, W. Wang, S. P. Feng, G. Chen, W. Liu, *Science* **2020**, *368*, 1091.
- [29] J. Duan, G. Feng, B. Yu, J. Li, M. Chen, P. Yang, J. Feng, K. Liu, J. Zhou, *Nat. Commun.* **2018**, *9*, 5146.
- [30] B. Guo, Y. Hoshino, F. Gao, K. Hayashi, Y. Miura, N. Kimizuka, T. Yamada, *J. Am. Chem. Soc.* **2020**, *142*, 17318.
- [31] C. Yang, Z. Suo, *Nat. Rev. Mater.* **2018**, *3*, 125.
- [32] B. Lu, H. Yuk, S. Lin, N. Jian, K. Qu, J. Xu, X. Zhao, *Nat. Commun.* **2019**, *10*, 1043.
- [33] M. Hua, S. Wu, Y. Ma, Y. Zhao, Z. Chen, I. Frenkel, J. Strzalka, H. Zhou, X. Zhu, X. He, *Nature* **2021**, *590*, 594.
- [34] M. Ding, L. Jing, H. Yang, C. E. Machnicki, X. Fu, K. Li, I. Y. Wong, P. Y. Chen, *Mater. Today Adv.* **2020**, *8*.
- [35] Q. Liu, G. Nian, C. Yang, S. Qu, Z. Suo, *Nat. Commun.* **2018**, *9*, 846.
- [36] A. S. Kurian, H. Souri, V. B. Mohan, D. Bhattacharyya, *Sens. Actuators, A* **2020**, *312*.
- [37] A. S. Kurian, V. B. Mohan, H. Souri, J. Leng, D. Bhattacharyya, *J. Mater. Res. Technol.* **2020**, *9*, 15621.
- [38] H. Souri, H. Banerjee, A. Jusufi, N. Radacsi, A. A. Stokes, I. Park, M. Sitti, M. Arnjadi, *Adv. Intell. Syst.* **2020**, *2*, 2000039.
- [39] P. Yang, H. Fan, *Chem. Res. Chin. Univ.* **2020**, *36*, 420.
- [40] T. Ding, L. Zhu, X.-Q. Wang, K. H. Chan, X. Lu, Y. Cheng, G. W. Ho, *Adv. Energy Mater.* **2018**, *8*, 1802397.
- [41] L. Yuan, X. Xiao, T. Ding, J. Zhong, X. Zhang, Y. Shen, B. Hu, Y. Huang, J. Zhou, Z. L. Wang, *Angew. Chem., Int. Ed. Engl.* **2012**, *51*, 4934.
- [42] G. Zhao, K. Rui, S. X. Dou, W. Sun, *Adv. Funct. Mater.* **2018**, *28*, 1803291.
- [43] C. Cheng, H. J. Fan, *Nano Today* **2012**, *7*, 327.
- [44] T. Sun, B. Zhou, Q. Zheng, L. Wang, W. Jiang, G. J. Snyder, *Nat. Commun.* **2020**, *11*, 572.